Human Myeloperoxidase: Structure of a Cyanide Complex and Its Interaction with Bromide and Thiocyanate Substrates at 1.9 Å Resolution†

Merilyn Blair-Johnson, Tristan Fiedler, and Roger Fenna*

Department of Biochemistry and Molecular Biology, University of Miami School of Medicine, P.O. Box 016129, Miami, Florida 33101

Received June 7, 2001; Revised Manuscript Received September 7, 2001

ABSTRACT: The 1.9 Å X-ray crystal structure of human myeloperoxidase complexed with cyanide ($R = 0.175$, $R_{free} = 0.215$) indicates that cyanide binds to the heme iron with a bent Fe−C−N angle of ∼157°, and binding is accompanied by movement of the iron atom by 0.2 Å into the porphyrin plane. The bent orientation of the cyanide allows the formation of three hydrogen bonds between its nitrogen atom and the distal histidine as well as two water molecules in the distal cavity. The 1.85 Å X-ray crystal structure of an inhibitory complex with thiocyanate ($R = 0.178$, $R_{free} = 0.210$) indicates replacement of chloride at a proximal helix halide binding site in addition to binding in the distal cavity in an orientation parallel with the heme. The thiocyanate replaces two water molecules in the distal cavity and is hydrogen bonded to Gln 91. The 1.9 Å structures of the complexes formed by bromide ($R = 0.215$, $R_{free} = 0.270$) and thiocyanate ($R = 0.198$, $R_{free} = 0.224$) with the cyanide complex of myeloperoxidase show how the presence of bound cyanide alters the binding site for bromide in the distal heme cavity, while having little effect on thiocyanate binding. These results support a model for a single common binding site for halides and thiocyanate as substrates or as inhibitors near the δ-meso carbon of the porphyrin ring in myeloperoxidase.

Myeloperoxidase (donor, hydrogen peroxide oxidoreductase, EC 1.11.1.7), MPO,[1] is one of the major enzymes of the antimicrobial system of mammalian neutrophils (*1*, *2*). The microbicidal activity of MPO is due to its ability to catalyze the peroxide-dependent oxidation of halide ions and thiocyanate to hypohalous acids and hypothiocyanate (*3*−*5*), which are effective antimicrobial agents (*6*, *7*). Reactive species produced by the catalytic activity of MPO are also thought to contribute to tissue damage associated with certain inflammatory diseases (*8*).

MPO is a dimer of 140 kDa, each half consisting of two polypeptide chains of 108 (light chain) and 466 (heavy chain) amino acids, a heme group, at least three sites of asparagine-linked glycosylation, and a bound calcium ion (*9*−*11*). The three-dimensional structure of canine MPO at 3 Å resolution revealed that the two halves of the dimer are apparently identical, and related by a dyad axis (*11*). There is one interchain disulfide bond at Cys 153 which links the two halves of the dimer, and cleavage of this disulfide yields a catalytically active hemienzyme (*9*, *11*). Additionally, there are six intrachain disulfides, five in the heavy chain and one in the light. The overall structure of the enzyme is predominantly α-helical and organized into locally folded domains about a heme core. Structure determination of human MPO at 2.3 Å and more recently 1.8 Å has established that the heme is a derivative of protoporphyrin IX in which the methyl groups on pyrrole rings A and C have been modified to allow ester formation with the carboxyl groups of Glu 242 and Asp 94, while the vinyl group on pyrrole ring A forms a sulfonium ion linkage with the sulfur atom of Met 243 (*12*−*14*).

The peroxidation of halides is a multistep reaction which begins with the two-electron oxidation of the enzyme by hydrogen peroxide to form Compound I, which contains a porphyrin π-cation radical with a ferryl (+IV) iron liganded to oxygen (*15*−*17*). MPO Compound I can carry out the two-electron oxidation of halides or thiocyanate in addition to the single-electron oxidation of a wide variety of aromatic alcohols and amines. Chloride has generally been considered to be the primary physiological substrate because it is present at high concentrations in the plasma (100−140 mM), relative to the concentrations of the other halides (<1−20 mM) (*18*, *19*). Kinetic analyses of the MPO-catalyzed peroxidation of chloride ions have revealed that the reaction occurs over a broad pH range and that the rate is affected by the relative concentrations of Cl^-, H_2O_2, and H^+ (*4*, *5*, *20*−*22*). High concentrations of Cl^- and H^+ inhibit the reaction in a manner that is competitive with respect to H_2O_2. Similar kinetics have been reported for the MPO-catalyzed oxidation of SCN^- to HOSCN (*23*). Recently, it has been shown that SCN^- is likely to be a significant physiological substrate for MPO, and reaction kinetic studies have shown that SCN^- is more effective than any of the halides as a donor of an electron to MPO Compound I (*24*, *25*).

Studies on the binding of halides and SCN^- to MPO have reached differing conclusions concerning the number of

† This work was supported by National Institutes of Health Grant GM 49149 to R.E.F.

* To whom correspondence should be addressed. E-mail: Rogfenna@Netscape.net. Phone: (305) 243-6564. Fax: (305) 243-3065.

[1] Abbreviations: MPO, myeloperoxidase; EPR, electron paramagnetic resonance; PEG, polyethylene glycol; NMR, nuclear magnetic resonance.

10.1021/bi0111808 CCC: $20.00
Published on Web 10/24/2001

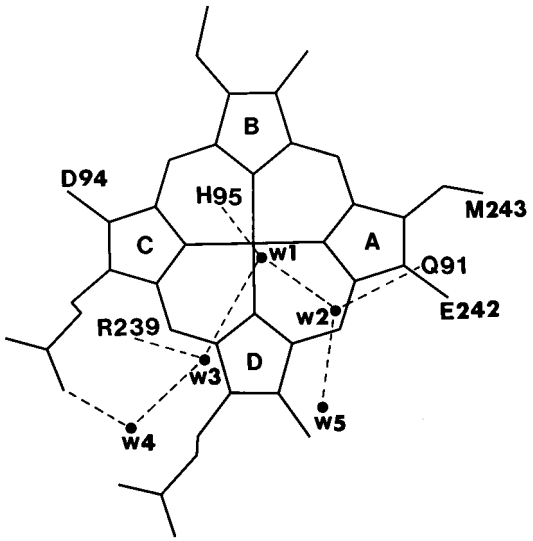

FIGURE 1: Diagram showing the arrangement of the five water molecules (W1−W5) in the distal heme cavity of human myeloperoxidase. The view is approximately normal to the heme plane. W1 is H-bonded to His 95 Nϵ, W2 to Gln 91 Nϵ, W3 to Arg 239 NH2, W4 to the heme propionate, and W5 has no additional hydrogen bonding. This figure also shows that the putative halide substrate binding site at W2 is positioned above the δ-methine bridge carbon between pyrrole rings A and D.

distinct sites and whether binding as a substrate and as an inhibitor involves the same or separate sites on the enzyme. The recently determined crystal structure of an MPO−bromide complex at 1.8 Å resolution has revealed four halide binding sites in each half of the molecule (*14*). Two are on the surface of the protein, well away from the heme; a third is at the amino terminus of the helix containing the proximal His 336, and a fourth is inside the distal heme cavity replacing a water molecule (W2) which is hydrogen bonded to the side chain of Gln 91 (Figure 1). It was proposed that halide binding at the distal cavity site inhibits the enzyme by interfering with the deprotonation of H_2O_2 by the adjacent distal His 95, a mechanism consistent with previous reports that inhibition by halides is competitive with respect to H_2O_2. The same distal cavity location in the Compound I form of the enzyme may also be the binding site for halide substrates, since it would allow for direct contact with the oxyferryl oxygen (*14*).

It has been suggested that the cyanide complex of MPO may be a useful analogue of Compound I for studies of halide substrate binding. It was shown by Lee et al. (*26*) that, at pH 4, the low-spin EPR spectrum of the cyanide complex is altered by halide binding and that the effects of chloride differ substantially from those of bromide or iodide. In this paper, we describe the X-ray crystal structure of an MPO−cyanide inhibitory complex and investigate its interaction with bromide and thiocyanate substrates.

MATERIALS AND METHODS

Crystallization. MPO isoform c was purified and crystallized as described previously (*27*, *28*). Crystals of human MPO crack when exposed to micromolar concentrations of cyanide. However, cocrystallization in the presence of 1 mM sodium cyanide at pH 5.5, under the same conditions used to crystallize the native enzyme, yielded crystals suitable for X-ray diffraction. Crystals of the MPO−SCN complex were prepared by equilibrating crystals of native MPO with a pseudo-mother liquor solution composed of 16% (w/v) polyethylene glycol (PEG) 8000, 50 mM ammonium sulfate (AMS), 50 mM sodium acetate, 2 mM calcium acetate, and 50 mM sodium thiocyanate at 22 °C and pH 5.5 for 24 h. Crystals of the MPO−CN−SCN double complex were obtained by soaking crystals of the cyanide complex in substitute mother liquor with the composition described above, with 1 mM sodium cyanide. Crystals of the MPO−CN−Br double complex were prepared similarly, except that 50 mM sodium bromide was substituted for SCN^- and the pH was reduced to 4.0. The pH reduction was achieved by stepwise equilibration of crystals of the cyanide complex with substitute mother liquor solutions at decreasing pHs from 5.5 to 4.0.

Data Collection, Structure Determination, and Refinement. Prior to being flash-frozen in a stream of gaseous nitrogen at −189 °C, crystals were briefly washed in substitute mother liquor containing 20% (v/v) 2-methyl-2,4-pentanediol as a cryoprotectant. All diffraction data were collected with a Rigaku RU300 X-ray generator equipped with a 30 cm MAR image plate detector, double-focusing mirrors, and a cryogenic temperature apparatus. Recorded data were indexed, integrated, scaled, and merged using the DENZO/SCALEPACK data processing software (*29*). Difference Fourier techniques were used to determine the structures of all four complexes. The 1.8 Å resolution atomic model of native human MPO [R = 19.7%, R_{free} = 23.9%, and good stereochemistry (Protein Data Bank, 1CXP)] served as the starting model for structure determination of both the MPO−CN and the MPO−SCN complexes. Following refinement, the atomic model of the cyanide complex was used as the phasing model to determine the structures of the MPO−CN−SCN and MPO−CN−Br double complexes.

Positions of bound cyanide ions were located from a difference Fourier map using $F_{o(MPO-CN)}$ and $F_{c(MPO)}$ as coefficients. The phasing model that was used was the coordinate set for native human MPO with a single water molecule (W1) located between the heme iron and the distal His 95 removed. Six water molecules and the chloride ion were removed from the native MPO model prior to calculation of structure factors used in phasing the $F_{o(MPO-SCN)} - F_{c(MPO)}$ difference Fourier map. These water molecules included W1−W5, in the distal heme cavity (Figure 1), and W601, associated with the bound chloride ion. Positions of bromide ions were located from a difference Fourier map using $F_{o(MPO-CN-Br)}$ and $F_{c(MPO-CN)}$ as coefficients. Since bromide is much more electron-dense than the other ligands being studied, and would therefore be evident as positive density in a difference map if it replaced either water or cyanide, it was considered unnecessary to remove any water molecules from the MPO−CN phasing model. However, water molecules W2−W4, together with the bound chloride and its associated water molecule, W601, were removed from the phasing model for the difference Fourier map calculated using $F_{o(MPO-CN-SCN)}$ and $F_{c(MPO-CN)}$ as coefficients.

Following inclusion of the ions located from the difference Fourier maps, each model was refined using X-PLOR version 3.85 (*30*) and stereochemical parameters derived from Engh and Huber (*31*). Simulated annealing was performed, using a starting temperature of 2000 °C, followed by 60 cycles of energy minimization. Noncrystallographic symmetry re-

Table 1: Data Collection and Refinement Statistics

	MPO−CN		MPO−SCN		MPO−CN−SCN		MPO−CN−bromide	
	total	(outer shell)	total	(outer shell)	total	(outer shell)	total	(outer shell)
resolution (Å)	50.0−1.90	(1.97−1.90)	50.0−1.85	(1.90−1.85)	30.0−1.90	(1.97−1.90)	50.0−1.90	(1.97−1.90)
no. of measurements	258017		396112		240861		343921	
no. of unique reflections	97701		108318		95064		92679	
I/σ	11.6	(6.4)	14.5	(9.7)	14.9	(6.1)	14.1	(7.9)
% completion	98.7	(97.5)	99.9	(99.8)	94.6	(90.6)	92.3	(89.8)
R_{merge}	0.060	(0.196)	0.048	(0.139)	0.057	(0.193)	0.061	(0.191)
refinement resolution (Å)	30.0−1.90	(1.97−1.90)	30.0−1.85	(1.93−1.85)	30.0−1.90	(1.99−1.90)	30.0−1.90	(1.97−1.90)
R-factor	0.172	(0.225)	0.181	(0.241)	0.193	(0.261)	0.215	(0.271)
R_{free} (5% data)	0.215	(0.266)	0.212	(0.251)	0.235	(0.293)	0.270	(0.302)
rmsd for bond lengths (Å)	0.010		0.011		0.010		0.013	
rmsd for bond angles (deg)	1.171		1.223		1.718		1.279	

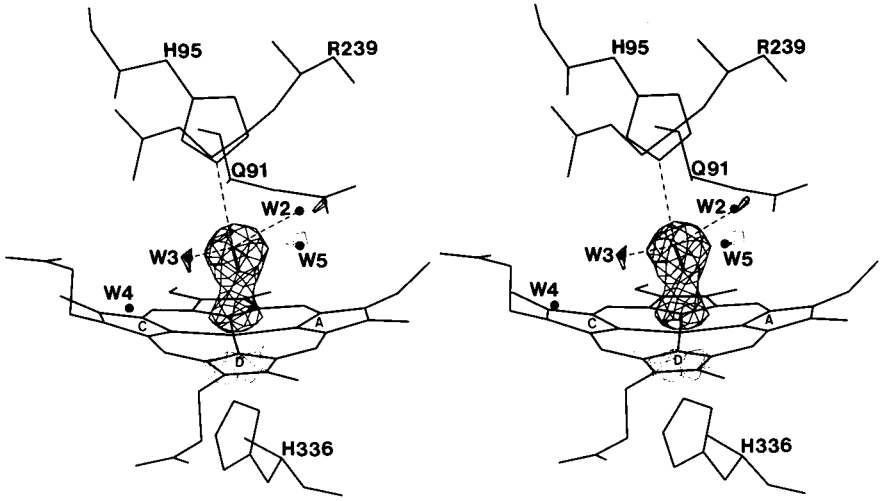

FIGURE 2: Stereodiagram showing the refined position of the bound cyanide ion superimposed on the $F_{o(MPO-CN)} - F_{c(MPO)}$ difference Fourier map. The map is contoured at $\pm 4\sigma$. Negative contours are shown with thinner lines. Positive and negative density above and below the heme indicate movement of the iron into the heme plane. The cyanide is inclined toward water molecules W2 and W3 with which it forms hydrogen bonds as well as with the distal His 95 Nϵ atom.

straints were not applied during refinement. In each case, residual maps were calculated following refinement to detect any additional significant unmodeled density, and the stereochemical parameters for all four models were analyzed using the program PROCHECK (*32*).

RESULTS

Structure of the MPO−Cyanide Complex. Flash-frozen crystals of native human MPO belong to space group $P2_1$, with a single MPO dimer in the asymmetric unit, and have the following unit cell dimensions: $a = 110.0$ Å, $b = 63.4$ Å, $c = 92.2$ Å, and $\beta = 97°$. Frozen crystals of the MPO−CN complex are closely isomorphous with the native having the following cell dimensions: $a = 111.2$ Å, $b = 63.5$ Å, $c = 92.3$ Å, and $\beta = 97.4°$. Data collection and scaling statistics are presented in Table 1. The major features of the difference Fourier map were confined to the immediate vicinity of the heme iron in each half of the molecule. An elongated positive peak, with a maximum density of 9.3σ (density values given are the averages of density maxima in the two halves of the molecule) on the distal side of the heme iron, together with a spherical negative peak, with a minimum density of -5.8σ on the proximal side, were interpreted as cyanide binding to the heme iron accompanied by a small shift of the iron atom into the plane of the heme (Figure 2). During refinement, the heme iron moved 0.2 Å into the heme plane from its position in the native enzyme. Because the porphyrin ring is considerably distorted from planarity, it is impractical to define an iron position with respect to a heme plane; however, in the cyanide complex, the iron refined to a position along the line connecting the nitrogen atoms of pyrrole rings B and D, whereas in the native enzyme, it was located 0.2 Å to the proximal side of this line. The refined heme iron to cyanide carbon distance of 2.06 Å is significantly shorter than the distance of 3 Å between the iron and the oxygen of W1 in the native enzyme. Cyanide binding displaces the water molecule (W1) which is hydrogen bonded to the distal His 95 in the native enzyme. As shown in Figure 2, the cyanide is inclined toward water molecules W2 and W3, with which it forms hydrogen bonds, giving Fe−C−N angles of 167° (A half) and 148° (B half). The orientation of the cyanide ion therefore appears to be determined by the formation of three hydrogen bonds between its nitrogen atom and the distal histidine as well as water molecules W2 and W3. Distances for these interactions are presented in Table 2. There do not appear to be any significant protein conformational changes associated with cyanide binding. Water molecule W2 shifts by ~0.5 Å away from the cyanide nitrogen, and a compensatory shift in water W5 maintains the hydrogen bond between these two water molecules.

Structure of the MPO−Thiocyanate Complex. Flash-frozen crystals of the MPO−SCN complex have cell dimensions ($a = 111.2$ Å, $b = 63.9$ Å, $c = 92.6$ Å, and $\beta = 97.5°$) that are sufficiently close to those of the native to allow

Table 2: Cyanide Interactions

		distance (Å)					
		MPO−CN		MPO−CN−Br		MPO−CN−SCN	
from	to	A	B	A	B	A	B
CN^- [C]	Fe	2.06	2.06	2.06	2.01	2.01	2.02
CN^- [N]	H95 Nϵ	2.68	2.86	2.98	2.71	2.68	2.63
CN^- [N]	W2	2.94	2.74	3.21	2.90		
CN^- [N]	W3	2.92	2.86	2.98	2.71	3.16	3.15
CN^- [N]	SCN^- [N]					3.08	2.75
Fe−C−N angle (deg)		167	148	120	132	151	160

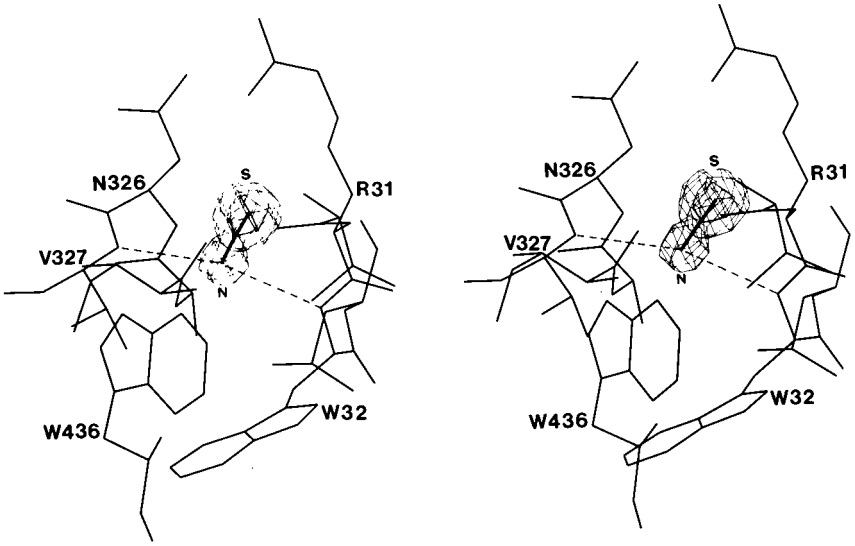

FIGURE 3: Stereodiagram showing the refined model of the MPO−SCN complex superimposed on the SCN^- difference Fourier map at the proximal helix halide binding site. The map is contoured at 6σ and 12σ. The SCN^- nitrogen is hydrogen bonded to the peptide NH groups of Trp 32 and Val 237.

calculation of a difference Fourier map, using $F_{o(MPO-SCN)}$ and $F_{c(MPO)}$ as coefficients. This map showed two elongated, pear-shaped peaks, indicative of SCN^- binding in each half of the MPO molecule, as well as three spherical peaks, corresponding to three water molecules in the distal heme cavity. As shown in Figure 3, pear-shaped density at the position of the bound chloride ion in the native enzyme with maxima of 17.0σ at one end and 10.2σ at the other clearly indicated the orientation of a bound thiocyanate ion. A second pear-shaped peak was located in the distal heme cavity with density of 13.8σ at one end and 6.8σ at the other, again clearly indicating the orientation of the bound thiocyanate. There was no indication of thiocyanate binding at the surface halide binding sites. In the absence of halides, these sites appear to be occupied by water molecules. The three spherical peaks in the distal heme cavity had densities of 6σ, 9σ, and 7σ, corresponding to water molecules W1, W3, and W4, respectively, which had been removed from the phasing model (Figure 4). The two thiocyanate ions and three water molecules in each half of the molecule were added to the model, and refinement was carried out. The occupancies of both thiocyanate ions refined to 1.0, and residual maps showed no further significant features in these regions. The crystallographic *R*-factor for the final structure was 0.178 (R_{free} = 0.210) for X-ray data to 1.85 Å resolution. Details of the data collection and refinement statistics are given in Table 1.

At the proximal helix halide binding site, both the chloride ion, found in the native enzyme structure, and its associated water molecule (W601) were replaced by the thiocyanate ion. The thiocyanate nitrogen occupies the chloride position, making electrostatic interactions with the peptide amide NH groups of Trp 32 and Val 327, while the sulfur replaces W601, making van der Waals interactions with the side chains of Leu 430, Trp 436, and Arg 31. To accommodate the larger sulfur atom in place of W601, the side chain of Arg 31 undergoes a significant conformational change. The Cδ and Nϵ atoms of Arg 31 move 0.8 and 0.6 Å away from the sulfur, respectively, while the Cβ, Cγ, and Cz atoms move 0.6, 0.8, and 0.3 Å closer, respectively. In the altered conformation, the Cβ, Cγ, and Cδ atoms of Arg 31 are all in van der Waals contact with the sulfur at distances of 3.9−4.0 Å. On the other side of the sulfur, the polypeptide backbone comprising residues Leu 33 and Pro 34 moves ~0.3 Å away, increasing the distance between the Leu 33 peptide carbonyl oxygen and the sulfur from 2.9 to 3.3 Å.

In the distal heme cavity, the thiocyanate ion lies almost parallel with the plane of the heme replacing water molecules W2 and W5 in the native enzyme. The nitrogen of SCN^-, at the W2 position, makes hydrogen bonds with the amide NH_2 of Gln 91 and water molecule W1 as well as a weak interaction with the Nϵ atom of the distal His 95 (Table 3), while the sulfur makes van der Waals contacts with Cγ of Glu 242, Cδ of Arg 239, and the heme pyrrole ring D methyl carbon. There do not appear to be any significant protein conformational changes associated with SCN^- binding at this location other than a small shift in the position of water molecule W1 of ~0.5 Å away from the SCN^- nitrogen.

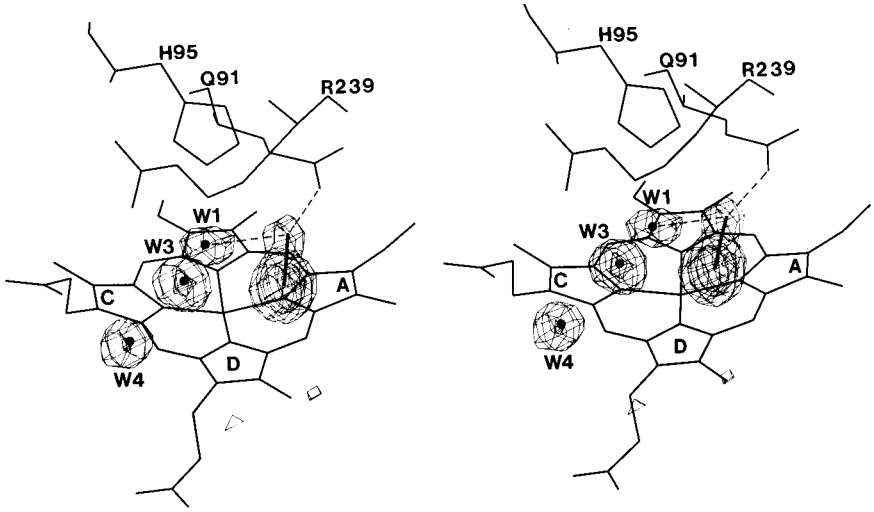

FIGURE 4: Stereodiagram showing the refined model of the MPO−SCN complex superimposed on the SCN^- difference Fourier map at the distal heme cavity. The map is contoured at $\pm 4\sigma$. The thiocyanate replaces water molecules W2 and W5. The nitrogen atom of SCN^- is hydrogen bonded to the Gln 91 NH_2 group and W1.

Table 3: Distal Cavity Thiocyanate and Bromide Interactions[a]

		distance (Å)	
from	to	A	B
Thiocyanate Complex, Distal Cavity Thiocyanate			
Gln 91 Nϵ		2.95	2.98
His 95 Nϵ	SCN^- N	(3.45)	(3.32)
W1 OH	SCN^- N	3.09	3.01
Cyanide−Bromide Complex, Distal Cavity Bromide			
W2 OH	Br^-	3.01	3.34
W4 OH	Br^-	(3.39)	(3.42)
Cyanide−Thiocyanate Complex, Distal Cavity Thiocyanate			
Gln 91 Nϵ	SCN^- N	3.16	3.15
His 95 Nϵ	SCN^- N	(3.40)	(3.19)

[a] Parentheses indicate weak or non-H-bonding interaction.

Bromide Binding to the MPO−Cyanide Complex. The structure of the MPO−CN−Br complex was determined at pH 4, corresponding to the conditions used in the spectroscopic studies of this complex in ref *10*. Crystals of the MPO−cyanide complex soaked in 50 mM sodium bromide and flash-frozen at −180° C have cell dimensions (a = 111.3 Å, b = 63.3 Å, c = 92.3 Å, and β = 97.4°) very similar to those of the cyanide complex described above. Data collection and scaling statistics for the 1.9 Å resolution data set collected from a single crystal are given in Table 1. The strongest features of the $F_{o(MPO-CN-Br)} - F_{c(MPO-CN)}$ difference map are found at the proximal helix halide binding site, where a peak of 20.4σ at the chloride ion position indicates its replacement by bromide. Two additional bromide binding sites on the surface of the molecule are partially occupied in this complex. Water molecule 758 has additional positive density at 9.8σ, while the surface-bound cyanide at the position of water molecule 889 in the native enzyme has additional density at 10.7σ. Both of these sites have previously been shown to bind bromide when crystals of the native enzyme were soaked in 50 mM bromide at pH 5.5 (*14*).

As shown in Figure 5, the difference map also indicates bromide binding in the distal cavity. Positive density at 5.8σ close to the position of water molecule W5 indicates partial replacement of this water by bromide. Significantly, the map shows no features (even at $\pm 1\sigma$) near water molecule W2, which was found to be the site of bromide binding in the distal cavity of the native enzyme. Refinement of the structure of the MPO−CN−Br complex resulted in an R-factor of 0.215 (R_{free} = 0.270) for X-ray data in the 30−1.9 Å range and good overall stereochemistry for the protein model (Table 1). Average occupancies at each of the bromide sites were determined to be 1.0 for the proximal helix halide binding site, 0.68 at the W889 surface site, 0.60 at the W758 surface site, and 0.51 at the W5 site in the distal heme cavity. The first three of these sites have occupancies similar to those observed when native MPO crystals were soaked in 50 mM bromide at pH 5.5 (*14*). On the other hand, the presence of bound cyanide appears to influence the binding of bromide in the distal cavity, where water molecule W5 is replaced, rather than water molecule W2, as seen in the native enzyme.

The refined position of the distal cavity bromide ion is 0.5 Å from the position previously occupied by water molecule W5 in the MPO−CN complex. The bromide does not appear to make any readily identifiable electrostatic interactions with the protein, the heme, or the bound cyanide. The closest protein atoms are the Cγ atom of Glu 242 (3.8 Å) and the Cγ atom of Arg 239 (3.8 Å); the nearest neighboring heme atom is the pyrrole ring D methyl carbon (4.55 Å), and the distance to the cyanide nitrogen is 5.4 Å. The only significant electrostatic interactions appear to be with water molecules W2 and W4 (Table 3). Superposition of the refined MPO−CN−Br model onto that of the MPO−CN model indicates a small change in the position of the Glu 242 ester linkage oxygen by ~0.3 Å away from the bound halide. However, as seen in Figure 5, there is a marked change in the orientation of the cyanide ion, which is significantly more tilted with respect to the normal to the heme plane with Fe−C−N angles of 120° and 132° in the two halves of the molecule compared with values of 167° and 148°, respectively, in the cyanide complex.

Thiocyanate Binding to the MPO−Cyanide Complex. Crystals of the MPO−CN complex soaked in thiocyanate have unit cell dimensions (a = 111.3 Å, b = 63.8 Å, c = 92.6 Å, and β = 97.5°) comparable with those of the MPO−CN complex. The $F_{o(MPO-CN-SCN)} - F_{c(MPO-CN)}$ difference Fourier map exhibited pear-shaped peaks corresponding to

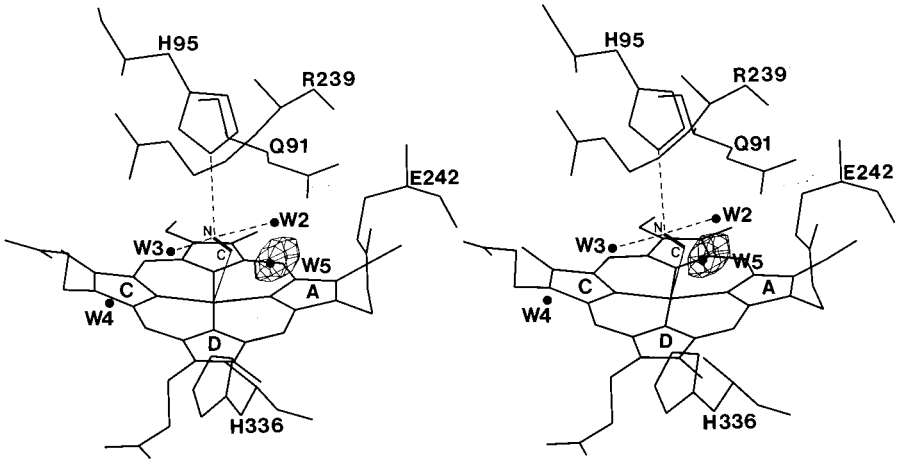

FIGURE 5: Stereodiagram showing the refined model of the MPO−CN−Br double complex superimposed on the $F_{o(MPO-CN-Br)} - F_{c(MPO-CN)}$ difference Fourier map. The map is contoured at $\pm 4\sigma$. All four water molecules in the distal cavity of the MPO−CN complex were included in the model. Additional positive density at the position of water molecule W5 indicates partial replacement by bromide. Although it is not indicated by significant features in the difference map, the orientation of the cyanide ion is altered from that shown in Figure 2.

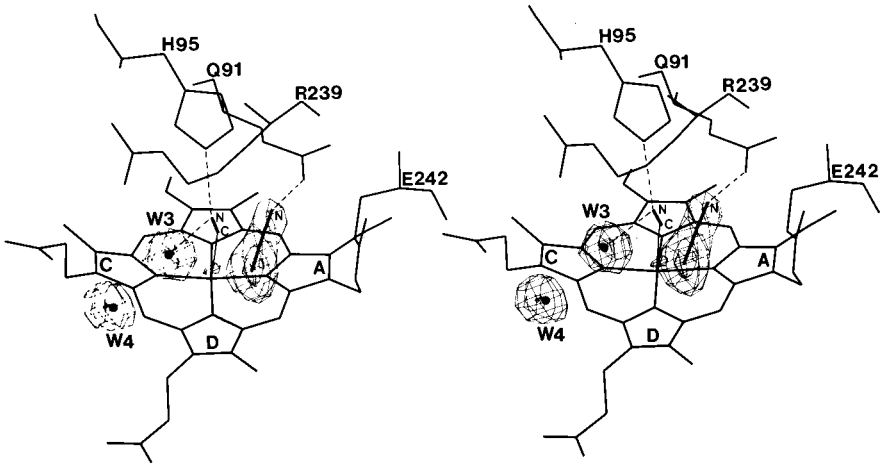

FIGURE 6: Stereodiagram showing the refined model of the MPO−CN−SCN complex superimposed on the $F_{o(MPO-CN-SCN)} - F_{c(MPO-CN)}$ difference Fourier map. The map is contoured at $\pm 4\sigma$. The thiocyanate replaces water molecules W2 and W5 and has a single hydrogen bond between its nitrogen and the amide group of Gln 91.

SCN^- binding at the same sites seen in the native MPO−SCN complex. The orientations of the SCN^- ions were again clearly indicated by sulfur to nitrogen electron density maxima ratios of 14.1σ:11.6σ at the proximal helix binding site and 9.1σ:5.5σ at the distal cavity site (Figure 6). Additional positive peaks of 8.4σ and 7.5σ in the distal cavity indicated the presence of water molecules W3 and W4, which had been removed from the phasing model. Occupancies of both thiocyanate ions refined to 1.0, as in the MPO−SCN complex.

The SCN^- ion in the distal cavity of the MPO−cyanide complex occupies the same position as in the native enzyme, except that it is inclined ~15° from its former orientation parallel with the heme. The cyanide ion orientation is virtually unchanged with an Fe−C−N angle of 155°, similar to that seen in the MPO−cyanide complex. However, whereas in the native enzyme the SCN^- nitrogen can form two hydrogen bonds with the amide NH_2 group of Gln 91 and water molecule W1, in the presence of cyanide only a single hydrogen bond with Gln 91 is possible. Since the cyanide nitrogen that replaces W1 is strongly hydrogen bonded to the Nϵ atom of the distal His 95, there is no available proton for simultaneous hydrogen bonding with the thiocyanate nitrogen.

Coordinates for all four of the structures described above, together with their respective sets of structure factors, have been deposited with the Protein Data Bank as entries 1D5L (MPO−CN), 1DNU (MPO−SCN), 1D7W (MPO−CN−Br), and 1DNW (MPO−CN−SCN).

DISCUSSION

Cyanide binding to MPO has previously been studied using a variety of spectroscopic techniques. The pH dependency of cyanide binding resembles that of H_2O_2, since both require the deprotonated form of a group with a pK_a of 4.0−4.3, presumed to be the distal histidine (*33*−*35*). Following deprotonation of HCN by the distal histidine, the CN^- anion binds to the heme iron to produce an $s = 1$ low-spin complex in which the cyanide nitrogen has been postulated to hydrogen bond to the protonated distal histidine (*36*, *37*). Movement of the iron atom by 0.2 Å into the heme plane is consistent with similar iron movement of 0.15 Å in cytochrome *c* peroxidase upon formation of a strong sixth ligand to a cyanide ion (*38*). Resonance Raman studies (*39*) have indicated a "bent" configuration for cyanide binding to MPO with an Fe−C−N angle of 155°, in good agreement with our finding of 157° for the average of angles measured from the two crystallographically independent subunits. It has been

suggested that the "bent" configuration could be due to a more constrained environment in the distal pocket of MPO, compared with horseradish peroxidase in which the angle was determined to be 170° (*39*). Our results support this hypothesis because the distance between the heme iron and the Nϵ atom of the distal His 95 is only 5.6 Å, which is too short to accommodate cyanide in an orientation normal to the heme plane, and would result in a short cyanide nitrogen to histidine nitrogen hydrogen bonding distance of ~2.3 Å. However, other hydrogen bonding considerations also appear to have a major influence on the orientation of the bound cyanide which is inclined toward the midpoint of a line linking water molecules W2 and W3. As a consequence, the cyanide nitrogen is able to form hydrogen bonds with both of these water molecules as well as the distal histidine (Table 2). A cyanide orientation normal to the heme plane would place the nitrogen too far from these water molecules to allow hydrogen bonding.

Previously, we had shown that the MPO substrate, bromide, binds to the enzyme, at both the proximal helix chloride binding site and a binding site, replacing water molecule W2 in the distal heme cavity (*14*). We have now shown that a second MPO substrate, thiocyanate, binds to the enzyme at these same two locations. At the proximal helix binding site, SCN^- replaces both the chloride and its associated water molecule, while in the distal cavity, it replaces two water molecules (W2 and W5). Thiocyanate has generally been considered to be the primary physiological substrate for the enzyme lactoperoxidase (LPO). Although the crystal structure of this enzyme has not been determined, sequence comparisons with MPO suggest that the heme environment is likely to be very similar (*11*), and the two enzymes exhibit similar kinetic properties when SCN^- is used as a substrate (*40*). NMR relaxation methods, using $S^{13}CN^-$ and $SC^{15}N^-$, have been applied by two groups to study the binding of SCN^- to bovine LPO. In both cases, it was determined that the nitrogen atom of SCN^- was located closer to the heme iron than the carbon atom. Iron to nitrogen and iron to carbon distances of 7.2 and 8.4 Å, respectively, were reported by Modi et al. (*40*), while much shorter distances of 2.7 and 3.5 Å, respectively, were later reported by Crull et al. (*41*). In our model of the MPO−SCN complex, the SCN^- nitrogen is also located closer to the iron than is the carbon with corresponding distances of 4.95 and 5.35 Å, close to the average of the previously reported sets of values.

The function of the anion binding site at the amino terminus of the proximal helix in MPO is not known. While a role in stabilizing the partial positive charge associated with the helix dipole moment is one possibility, a more direct role in catalysis cannot yet be discounted. The origin of the oxygen atom in the hypohalous acid or hypothiocyanate reaction product has not been experimentally determined. If this oxygen derives exclusively from H_2O_2, then peroxidation must presumably occur in the distal heme cavity, since it is known that the oxyferryl oxygen of Compound I in peroxidases originates from H_2O_2 (*42*). On the other hand, if this oxygen can be derived from water, then substrate peroxidation at sites remote from the distal cavity may be possible. For example, water molecule W601 could be considered a possible source of the oxygen atom for the peroxidation of either chloride or bromide at the proximal helix binding site, although an analogous reaction involving thiocyanate may be precluded since this water is displaced upon SCN^- binding to the enzyme and there are no other ordered water molecules closer than 7.5 Å. Precedence for such a mechanism has been established for cytochrome *c* peroxidase in which Compound I formation yields a tryptophan free radical on the proximal side of the heme (*43*, *44*). Also, the initial porphyrin π-cation radical of LPO Compound I is thought to convert rapidly to an oxyferryl protein radical in which two oxidizing equivalents are retained (*45*−*48*). Although two potential tryptophan radicals Trp 32 and Trp 436 are located very close to the halide binding site in MPO, there have been no reports of analogous protein free radicals associated with Compound I of MPO.

Since both Compound I and the cyanide complex of MPO contain six-coordinated low-spin $s = 1$ iron centers, it has been suggested that an MPO−CN complex might provide a useful model for Compound I, which is itself short-lived and hence difficult to study (*26*). A pH-dependent differential in the effects of chloride versus bromide or iodide on the anisotropy of the EPR spectrum of the low-spin MPO−CN complex has been observed. At pH 4, chloride induces a decrease in anisotropy, while both bromide and iodide give rise to an increase. At both pH 6 and 8, an increase in anisotropy is seen for all three halides. The authors note that the observed halide effects could arise from a change in the orientation of the Fe−CN bond with respect to the heme plane and/or a change in the σ-basicity of the bound cyanide and that steric effects due to the larger ionic radii of iodide and bromide compared with that of chloride could account for the differential effects of these ligands.

We have shown that the presence of bound cyanide results in a distinct change in the site of bromide binding to MPO and that bromide binding alters the orientation of the cyanide ion with respect to the heme plane by ~30°. In the native enzyme, bromide replaces water molecule W2, which is hydrogen bonded to the amide of Gln 91 in the proximity of the Nϵ atom of the distal His 95, but in the cyanide complex, W2 is not displaced and bromide binds in place of W5. The reason for this change appears to be the inaccessibility of the W2 site to an ion as large as bromide when cyanide is bound to the iron. When a bromide ion is modeled at the W2 position in the MPO−CN complex, three simultaneous close contacts of 3.3 Å are made with the cyanide nitrogen, the Cγ atom of Glu 242, and the Cδ atom of Arg 239. This distance is significantly shorter than the sums of the van der Waals radii of the atoms in contact (3.45 Å for nitrogen and bromide and 3.65 Å for carbon and bromide). Accommodation of the bromide ion by movement of any of these atoms appears to be unfavorable, because the position of the cyanide nitrogen is influenced by the formation of three hydrogen bonds, the Cγ atom of Glu 242 is constrained by the geometry of the ester linkage between this residue and the heme, and the guanidinium group of Arg 239 forms a salt bridge with the carboxyl group of Asp 98. In contrast, the presence of bound cyanide has little effect on the binding of SCN^-, where the smaller nitrogen atom of SCN^- can occupy the W2 position in both the native and cyanide-bound forms of the enzyme. Although no crystallographic studies have been reported for chloride binding in the distal cavity of MPO, it is possible that the W2 position could accommodate this ion equally well in both

native MPO and its cyanide complex since its ionic radius (1.81 Å) is significantly smaller than that of bromide (1.96 Å) or iodide (2.20 Å). The differential spectral effects of chloride versus bromide or iodide binding to the cyanide complex of MPO could therefore indeed be ascribed to steric effects resulting from the differing ionic radii of these ions.

Results from this study, together with previous observations of bromide binding in the distal cavity of native MPO (*14*), support a model in which halides and thiocyanate occupy the same site as inhibitors and substrates. When bound to the native enzyme, in place of water molecule W2, they interact with the distal histidine, thereby competitively inhibiting the binding of peroxide substrates and preventing the formation of Compound I. In contrast, binding at the same site, as substrates, in Compound I appears to be favorable for electron transfer to the heme and incorporation of the oxyferryl oxygen into the hypohalous acids and hypothiocyanate reaction products. It is noteworthy that this postulated substrate binding site is close to the δ-methine bridge carbon between pyrrole rings A and D. Single-electron transfer has been postulated to occur at the heme periphery in horseradish peroxidase (*49*), and this particular methine bridge carbon in MPO may be particularly electron deficient in Compound I since it is located adjacent to the positively charged sulfonium ion linkage to the vinyl group attached to pyrrole ring A. Thus, a possible mechanism for two-electron peroxidation of halides catalyzed by MPO could proceed via direct electron transfer to the δ-meso carbon of the porphyrin π-cation radical followed by incorporation of the oxyferryl oxygen into the hypohalous acid product.

ACKNOWLEDGMENT

We thank Mrs. Lan Wang for assistance with the purification of human MPO.

REFERENCES

1. Schultz, J., and Kaminker, K. (1962) *Arch. Biochem. Biophys. 96*, 465−467.
2. Salmon, S. E., Cline, M. J., Schultz, J., and Lehrer, R. I. (1970) *N. Engl. J. Med. 282*, 250−253.
3. Klebanoff, S. J. (1970) *Science 169*, 1095−1097.
4. Stelmaszynska, T., and Zgliczynski, J. M. (1974) *Eur. J. Biochem. 45*, 305−312.
5. Harrison, J. E., and Schultz, J. (1976) *J. Biol. Chem. 251*, 1371−1374.
6. Belding, M. E., Klebanoff, S. J., and Ray, C. G. (1970) *Science 167*, 195−196.
7. Agner, L. (1972) in *Structure and Function of Oxidation−Reduction Enzymes* (Akeson, K., and Ehrenberg, A., Eds.) pp 329−335, Pergamon Press, Oxford, U.K.
8. Weiss, S. J. (1989) *N. Engl. J. Med. 320*, 365−376.
9. Andrews, P. C., and Krinsky, N. I. (1981) *J. Biol. Chem. 256*, 411−418.
10. Olsen, F. L., and Little, C. (1983) *Biochem. J. 209*, 781−787.
11. Zeng, J., and Fenna, R. E. (1992) *J. Mol. Biol. 226*, 185−207.
12. Fenna, R. E., Zeng, J., and Davey, C. A. (1995) *Arch. Biochem. Biophys. 316*, 653−656.
13. Taylor, K. L., Strobel, F., Yue, K. T., Ram, P., Pohl, J., Woods, A. S., and Kinkade, J. M., Jr. (1995) *Arch. Biochem. Biophys. 316*, 635−642.
14. Fiedler, T., Davey, C., and Fenna, R. (2000) *J. Biol. Chem. 275*, 11964−11971.
15. George, P. (1952) *Adv. Catal. 4*, 367−428.
16. Chance, B. (1952) *Arch. Biochem. Biophys. 37*, 235−237.
17. Dolphin, D., Forman, A., Borg, D. C., and Felton, R. H. (1971) *Proc. Natl. Acad. Sci. U.S.A. 68*, 614−618.
18. Wood, J. L. (1975) in *Chemistry and Biochemistry of Thiocyanic Acid and its Derivatives* (Newman, A. A., Ed.) pp 156−163, Academic Press, New York.
19. Holzbecher, J., and Ryan, D. E. (1980) *Clin. Biochem. 13*, 277−278.
20. Bakkenist, A. R. J., De Boer, J. E. G., Plat, H., and Wever, R. (1980) *Biochim. Biophys. Acta 613*, 337−348.
21. Andrews, P. C., and Krinsky, N. I. (1982) *J. Biol. Chem. 257*, 13240−13245.
22. Zgliczynski, J. M., Selvaraj, R. J., Paul, B. B., Stelmaszynska, T., Poskitt, P. K. F., and Sbarra, A. J. (1977) *Proc. Exp. Biol. Med. 154*, 418−422.
23. Wever, R., Kast, W. M., Kasinoedin, J. H., and Boelens, R. (1982) *Biochim. Biophys. Acta 709*, 212−219.
24. Van Dalen, C. J., Whitehouse, M. W., Winterbourn, C. C., and Kettle, A. J. (1997) *Biochem. J. 327*, 487−492.
25. Furtmuller, P. G., Burner, U., and Obinger, C. (1988) *Biochemistry 37*, 17923−17930.
26. Lee, H. C., Booth, K. S., Caughey, W. S., and Ikeda-Saito, M. (1991) *Biochim. Biophys. Acta 1076*, 317−320.
27. Sutton, B. J., Little, C., Olsen, R. L., and Willassen, N. P. (1988) *J. Mol. Biol. 199*, 395−396.
28. Davey, C. A., and Fenna, R. E. (1996) *Biochemistry 35*, 10967−10973.
29. Otwinowski, Z. (1993) Data Collection and Processing. In *Proceedings of the CCP4 Study Weekend* (Sawyer, L., Isaacs, N., and Bailey, S., Eds.) pp 56−62, Daresbury Laboratory, Warrington, England.
30. Brunger, A. T. (1992) *X-PLOR. A System for X-ray Crystallography and NMR. Version 3.1 Manual*, Yale University Press, New Haven, CT.
31. Engh, R. A., and Huber, R. (1991) *Acta Crystallogr. A47*, 392−400.
32. Laskowski, R. A., MacArthur, M. W., Moss, D. S., and Thornton, J. M. (1992) *PROCHECK V2: Programs to Check the Stereochemical Quality of Protein Structures*, Oxford Molecular Ltd., Oxford, England.
33. Bolscher, B. G. J. M., and Wever, R. (1984) *Biochim. Biophys. Acta 788*, 1−10.
34. Ikeda-Saito, M. (1985) *J. Biol. Chem. 260*, 11688−11692.
35. Ikeda-Saito, M. (1987) *Biochemistry 26*, 4344−4349.
36. Shiro, Y., and Morishima, I. (1986) *Biochemistry 25*, 5844−5849.
37. Thanabal, V., de Ropp, J. S., and La Mar, G. N. (1988) *J. Am. Chem. Soc. 110*, 3027−3035.
38. Edwards, S. L., and Poulos, T. L. (1990) *J. Biol. Chem. 265*, 2588−2595.
39. Lopez-Garriga, J. J., Oertling, W. A., Kean, R. T., Hoogland, H., Wever, R., and Babcock, G. T. (1990) *Biochemistry 29*, 9387−9395.
40. Modi, S., Behere, D. V., and Mitra, S. (1989) *Biochemistry 28*, 4689−4694.
41. Crull, G. B., and Goff, H. M. (1993) *J. Inorg. Biochem. 15*, 181−192.
42. Hewson, W. D., and Hagar, L. P. (1979) in *The Porphyrins* (Dolphin, D., Ed.) Vol. VIIB, p 295, Academic Press, New York.
43. Erman, J. E., Vitello, L. B., Mauro, J. M., and Kraut, J. (1989) *Biochemistry 28*, 7992−7995.
44. Yonetani, T., Schleyer, H., and Ehrenberg, A. (1976) *J. Biol. Chem. 241*, 3240−3242.
45. Kimura, S., and Yamazaki, I. (1979) *Arch. Biochem. Biophys. 198*, 580−588.
46. Hu, S., and Kincaid, J. R. (1991) *J. Am. Chem. Soc. 113*, 7189−7194.
47. Taurog, A., Dorris, M., and Doerge, D. R. (1994) *Arch. Biochem. Biophys. 315*, 82−89.
48. Lardinois, O. M., Medzihradszky, K. F., and Ortiz de Montellano, P. R. (1999) *J. Biol. Chem. 274*, 35441−35448.
49. Ator, M. A., and Ortiz de Montellano, P. R. (1987) *J. Biol. Chem. 262*, 1542−1551.

BI0111808